JOURNAL OF MATERIALS SCIENCE 31 (1996) 545–550

Microstructures and phase selection in rapidly solidified Zn–Mg alloys

M. V. AKDENIZ
Metallurgical Engineering Department, Middle East Technical University, Ankara, Turkey
J. V. WOOD
Department of Materials Engineering and Materials Design, University of Nottingham, Nottingham, UK

The Zn–Mg system has potential glass-forming ability, and therefore studies were made of rapidly solidified zinc-based Zn–Mg alloys containing up to 6 wt% Mg. These alloys exhibited interesting eutectic phase selections and structural transitions across the ribbon thickness which are represented on a microstructure selection diagram for rapid solidification conditions. Although rapid solidification is known in many cases to produce metastable phases, in this case the equilibrium eutectic mixtures of Zn–Mg_2Zn_{11} are observed after rapid solidification, whereas the metastable eutectic mixture Zn–$MgZn_2$ forms under normal solidification conditions. However, in the melt-spun Zn–Mg alloy which is exactly at eutectic composition, three different structures are observed across the ribbon thickness. These three structures do not exist simultaneously in the same region, but structural transitions occur as the thickness increases from the wheel side to the free side. Eutectic and hypereutectic alloys show a tendency to form a metallic glass. In these alloys a critical growth velocity exists beyond which eutectic solidification is not possible, suggesting a possible transition from eutectic solidification to amorphous phase formation. The eutectic phase selection and the extent to which a specific microstructure is present depends on the variation in growth rate and solid–liquid interface stability during rapid solidification.

1. Introduction

The dominant product phase in rapidly solidified microstructure is determined to a large extent by the undercooling below the respective melting points of competing phases during the nucleation stage and the competition between different modes of growth of the contending phases and constituents [1]. Because the growth conditions (i.e. growth rate, melt composition, and temperature gradient) determine the growth morphology and the resulting microstructure of the solidified alloy, the factors controlling the transition from one morphology to another could be important. The prediction of observed morphologies and the limits of occurrence of particular microstructures can be represented schematically by a microstructure selection diagram in the form of the growth velocity – alloy concentration, $V - C_0$, relationship. Recently, such diagrams for various alloy systems which solidify over the growth ranges 1–10 mm s^{-1} by the Bridgman technique and up to several metres per second by laser, electron or plasma-beam spraying, have been documented [2].

The zinc-rich Zn–Mg system was chosen for this investigation because the Zn–Mg system has potential glass-forming ability [3, 4] and the eutectic composition of the Zn–3 wt % Mg alloy has been found to solidify with more than one morphology [5]. This portion is known to exhibit competitive growth between two eutectic systems; a metastable eutectic between the phases $MgZn_2$ and Zn (EU1), and the stable eutectic consisting of the intermetallic compound Mg_2Zn_{11} and Zn (EU2). The eutectic structures of the zinc-rich Zn–Mg system have been described in detail [6–10] and the growth-rate dependent structural transitions have been demonstrated by an accelerated method [10] over the growth-rate range of 1×10^{-5}–5×10^{-5} cm s^{-1}. A solidification microstructure selection diagram has been determined recently for Zn–Mg alloys containing up to 4.5 wt % Mg over the growth velocity range 0.001–8 mm s^{-1} by means of the Bridgman technique, and the observed structural transitions have been explained on the basis of the competitive growth theory [5]. There has been considerable interest in determining the microstructure selection diagram of alloy systems under rapid solidification conditions because the formation of microstructures, phase selection and transition between the growth morphologies at high growth rates have become important in the development of novel alloys by the rapid solidification processes.

The purpose of this work was to examine the glass-forming ability of zinc-rich Zn–Mg alloys and to

0022–2461

report the formation of a variety of microstructures and structural transitions across the ribbon thickness which are represented by the microstructure selection diagram for rapid solidification conditions.

2. Experimental procedure

Fifteen Zn–Mg alloys were prepared in the range 0–6 wt % Mg from weighed portions of commercial purity zinc (99.98%) and magnesium (99.97%). Melting was undertaken in air using a mixed halide flux containing magnesium salts in a graphite crucible by means of r.f. induction heating. The alloys were then cast into a steel mould, and some of them were examined in the as-cast condition. The production of rapidly solidified material was achieved by the standard chill-block melt-spinning technique. Small pieces of material cut from the as-cast rod were remelted by means of r.f. induction heating in a stainless steel crucible with a 0.75 mm × 10 mm slot orifice coated with a thin layer of graphite. The wheel and crucible assembly were enclosed in a chamber which was initially evacuated to 10^{-2} Pa and double flushed with argon to prevent oxidation of material during melting and spinning. The temperature of the melt was monitored by inserting a thermocouple into the crucible. When the desired processing parameters were achieved, an argon back pressure of 1 MPa was applied to eject the melt on to a 254 mm diameter water-cooled copper wheel. A distance of 1.5 mm between the crucible and the wheel surface and wheel peripheral speed of 10 m s^{-1} were maintained for all experiments.

Owing to the extreme brittleness and very thin cross-section of some alloy compositions, only those ribbons with a reasonable ductility and thickness could be prepared for metallographic examination. Transmission electron microscopy was used to identify the precipitates present in rapidly solidified samples at an accelerating voltage of 200 kV. The transformation reaction temperatures of the alloys were determined on a differential scanning calorimeter (DSC) where the specimens were heated at a standard rate of 20 °C min^{-1} under a constant argon flow of 0.3 l min^{-1}. X-ray diffraction analysis was undertaken using Debye–Scherrer camera of 114.6 mm diameter in which, for rapidly solidified (RS) samples, 15 mm long thin strips cut from the as-spun ribbon, and for air cooled samples, powder obtained by filling, were exposed to iron-filtered CoK_α radiation operated at 40 kV with 20 mA for 6 h.

3. Results and discussion

In view of the possible T_0 configuration of the zinc-rich Zn–Mg system (Fig. 1), the observed microstructures may be explained by mapping the limits of occurrence of possible microstructures for various compositions and growth rates (Fig. 2). The phases in the zinc-rich portion of the phase diagram have a very narrow range of composition and thus also a narrow range of free energy curves preventing the T_0 curve becoming continuous [11, 12]. Therefore, the T_0

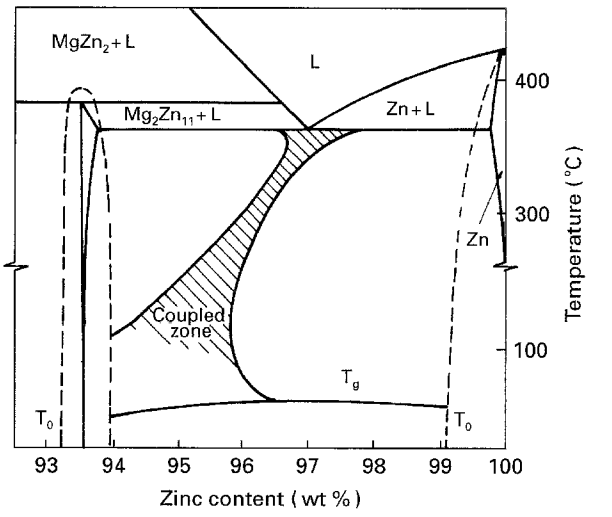

Figure 1 Possible T_0 configuration in the zinc-rich portion of the Zn–Mg system.

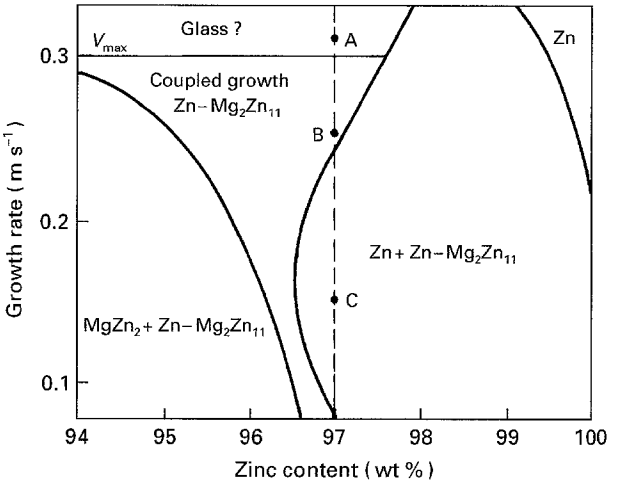

Figure 2 Schematic drawing of the growth rate–composition map of the zinc-rich Zn–Mg alloys.

curves will not extend far from the phases, and plunge to a very low temperature. This produces a rather wide range of alloy compositions between the T_0 curves of the zinc and Mg_2Zn_{11} phases which must crystallize as two-phase solids [13]. However, the coupled zone shifts from a symmetry position and is skewed towards the facet-forming Mg_2Zn_{11} side of the phase diagram. Alloys which exhibit asymmetric coupled zones also have asymmetric T_0 curves, so in this type of configuration very little extension of solubility is possible and alloys undergoing eutectic growth are strong candidates for glass formation [14].

The demarcation lines in Fig. 2 separate the regions where the different types of predicted microstructures exist, and the vertical line drawn at a particular alloy composition represents growth-rate changes during melt spinning. The estimated *average* growth rate of pure and dilute zinc alloy during melt spinning is $V \approx 0.1$ m s^{-1} [15]. This average value takes into account both the initial high-growth regime and the subsequent comparatively lower growth period during isothermal solidification [16]. The actual growth rate is predicted to be $V > 0.3$ m s^{-1} during the initial

period, and progressively reduces to a constant value of 0.1 $m\,s^{-1}$ when the isothermal solidification conditions are achieved.

Dilute Zn–Mg alloys (< 1 wt % Mg) exhibit planar solidification at the wheel side and fine, random zinc dendrites at the free surface of the ribbon (Fig. 3). These alloys exhibit an initial chill zone leading to columnar growth parallel to the heat flow direction. The dendritic like structures at the wheel side, which are parallel to the heat flow direction, actually occur as a result of a solid-state precipitation reaction both inside the grains and along the grain boundaries. Transmission electron microscopy (Fig. 4) reveals the details of the precipitates, and X-ray diffraction studies established that they are Mg_2Zn_{11}. In these alloys, solid solubility extension of the zinc-rich phase would be possible at high growth rates. However, due to a very low precipitation reaction temperature, the excess magnesium in supersaturated zinc solid solution precipitates as Mg_2Zn_{11}, and no solid solubility extension is observed (Fig. 5). As the growth rate reduces to a constant value where isothermal solidification starts, it crosses the demarcation line, and zinc dendrites plus interdendritic EU2 structure form at the free side of the ribbon. These alloys exhibit interface instability across the ribbon thickness at a particular growth condition, i.e. plane front solidification at the wheel side, cellular and dendritic solidification at the free side of the ribbon. Although alloys having intermediate compositions (3 > wt % Mg > 1) do not show any microstructural transition (Fig. 6), because there is no crossing of the demarcation line as the growth rate changes. The only salient feature is that primary zinc dendrites align parallel to the heat flow direction at the wheel side then become randomly distributed as the growth rate decreases towards the free side of the ribbon.

However, in the alloy which is exactly at the eutectic composition, three different structures were observed across the ribbon thickness; (i) a featureless zone with Mg_2Zn_{11} precipitates, (ii) fine cellular (EU2) eutectic structure, and (iii) primary zinc dendrite plus (EU2) interdendritic eutectic. Metallographic investigations showed that these three structures did not exist simultaneously in the same region, but for a given solidification condition a structural transition occurs either from (i) to (ii), (Fig. 7a), or from (ii) to (iii), (Fig. 7b), as the thickness increases from the wheel side to the free

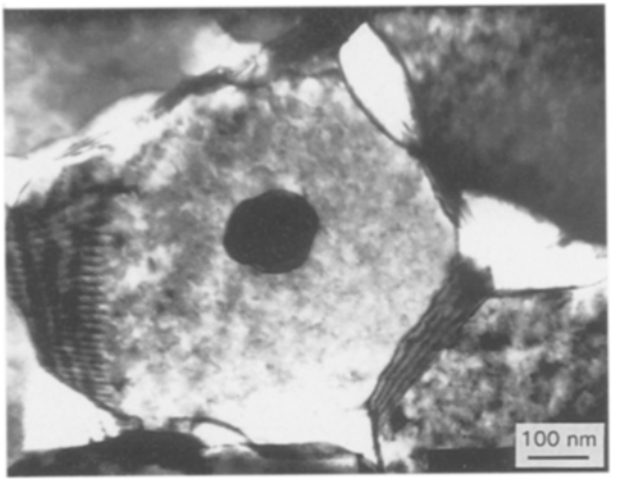

Figure 4 Transmission electron micrograph showing Mg_2Zn_{11} precipitates in rapidly solidified Zn–1 wt % Mg alloy.

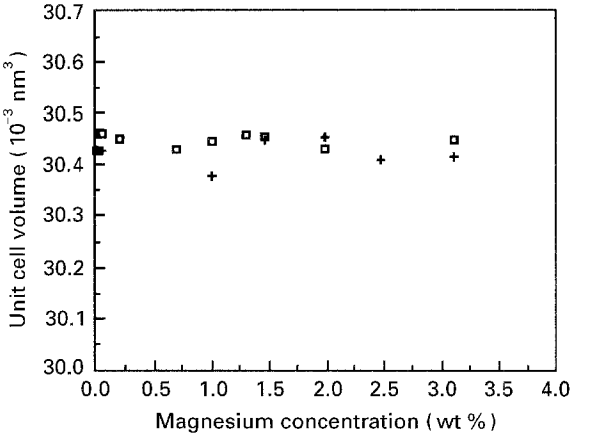

Figure 5 Unit cell volume of zinc solid solution as a function of magnesium concentration in (+) air cooled and (□) rapidly solidified samples.

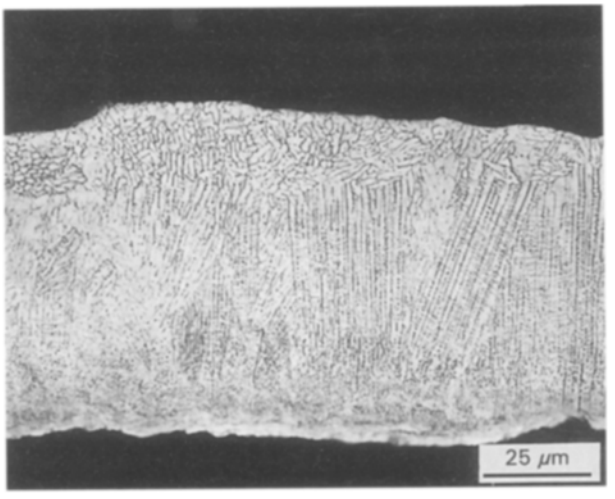

Figure 3 Optical micrograph of rapidly solidified Zn–0.5 wt % Mg alloy. Note the planar solidification at the wheel side and Mg_2Zn_{11} precipitates.

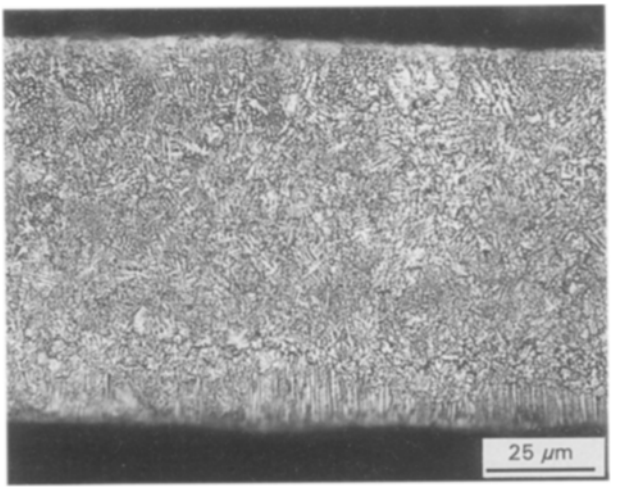

Figure 6 Optical micrograph of rapidly solidified Zn–1.98 wt % Mg alloy.

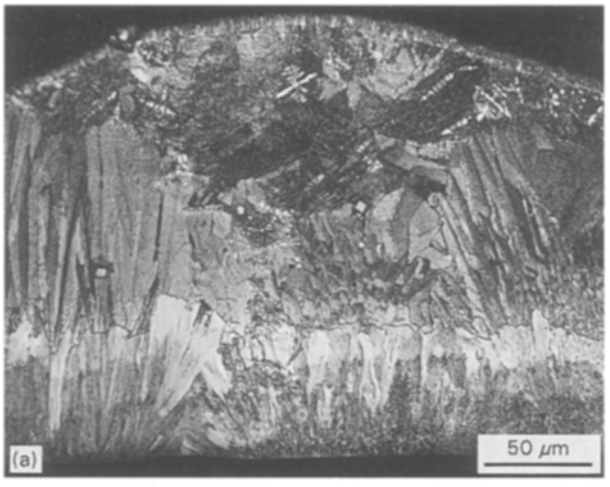

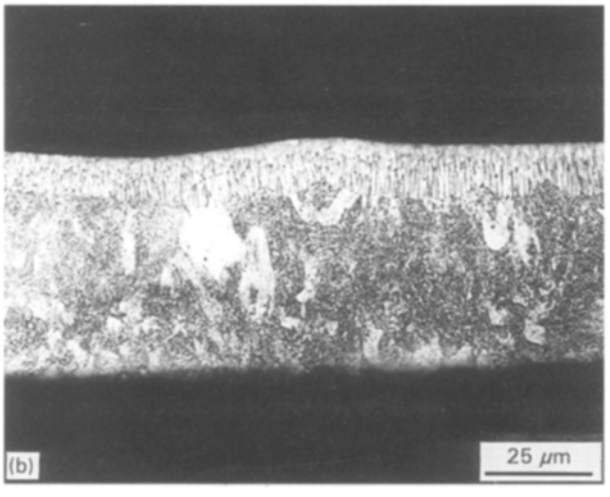

Figure 7 Optical micrographs of rapidly solidified Zn–3.11 wt % Mg eutectic alloy showing structural transitions (a) from the featureless zone with Mg_2Zn_{11} precipitates to the fine cellular EU2 structure, (b) from EU2 to primary zinc dendrites plus interdendritic EU2 structure. Note the well-defined band of zinc dendrites at the free side.

side. The selection and the extent of a specific microstructure depends on the local solidification conditions and the asymmetric nature of the coupled growth zone. When the eutectic alloy is highly undercooled, solidification starts at point *A* with a very high growth rate. However, it was pointed out that for high-speed eutectic growth, a maximum growth rate exists beyond which eutectic solidification could no longer occur because of temperature dependence of the solute diffusivity [12, 17, 18] and the values of partition coefficients approach unity [19]. Therefore, the actual growth rate at the beginning of solidification (i.e. at the wheel side) may exceed the maximum growth rate for eutectic solidification for this system ($V \approx 0.3\ m\,s^{-1} > V_{max}$). This results in the featureless zone at the wheel side of the ribbon, suggesting possible formation of an amorphous phase. Nevertheless, because of the very low crystallization temperature, the amorphous phase immediately crystallizes via the formation of Mg_2Zn_{11} precipitates. As the growth rate decreases with increasing ribbon thickness to a constant value, point *B*, the transition to the EU2 structure takes place. Point B may be situated very close to the demarcation line of the Zn + EU2 region and, if so, any fluctuation in the growth rate during solidification will shift its position away from the coupled zone into this region, and result in the formation of zinc dendrites within a eutectic matrix (Fig. 7a). If the alloy is insufficiently undercooled it cannot exceed the maximum eutectic growth rate ($V < 0.3\ m\,s^{-1}$). Thus, solidification starts at point B in the coupled zone allowing the formation of the EU2 structure at the wheel side. When the growth rate decreases to the point *C*, it eventually intersects the demarcation line and enters the Zn + EU2 region where structural transition from the coupled growth to the well-defined band of zinc dendrites plus interdendritic EU2 structures occurs at the free side of the ribbon (Fig. 7b). This transition is associated with the morphological single-phase instability of the zinc phase in the EU2 eutectic.

The hypereutectic alloys, especially alloy compositions close to the facet-forming Mg_2Zn_{11} phase, are particularly important in terms of glass formation. The Zn–Mg system has the greatest potential glass-forming ability [3, 4] and the first amorphous phase which consisted only of simple metals were made of Zn–Mg alloys in the narrow composition range around the eutectic point [3] in the magnesium-rich side of the phase diagram. Nevertheless, in the zinc-rich portion of the phase diagram, the coupled zone is asymmetrically disposed towards the faceted Mg_2Zn_{11} phase. Such shifts may also change the glass-forming ability of the alloy towards the compositions close to the Mg_2Zn_{11} phase. Consistent with this prediction, the present results showed that there is some evidence of possible formation of glassy structures at a composition around 6 wt % Mg. It seems likely that a limit of eutectic growth may exist and the transition from eutectic solidification to an amorphous phase is expected to occur due to the growth problems of the facet-forming Mg_2Zn_{11}. Although the presence of a residual amorphous phase could not be detected by X-ray diffraction due to extreme instability of the ribbon, the thermal behaviour of the alloy was similar to $Mg_{70}Zn_{30}$ metallic glass [3, 4] (Fig. 8). It is interesting to note that the exothermic reaction temperature at 130 °C which accounts, by X-ray diffraction analysis, for the formation of the Mg_2Zn_{11} phase in Zn–6 wt % Mg alloy is exactly the same as the crystallization temperature of Mg_7Zn_3 formed by decomposition of the $Mg_{70}Zn_{30}$ metallic glass. Moreover, both of the alloys have shown the weaker exothermic peak at a higher temperature but a low-temperature crystallization peak of the amorphous phase was not observed in this present investigation. These observations suggest that Zn–6 wt % Mg alloy has a very low crystallization temperature, presumably close to room temperature, which makes the alloy extremely unstable. Therefore, devitrification may take place shortly after melt spinning, causing initially shiny and reasonably ductile freshly produced ribbons to become extremely brittle and have a matt, dull appearance after a small period of time ($\sim$ 5–6 h) at room temperature, as was observed in this present investigation.

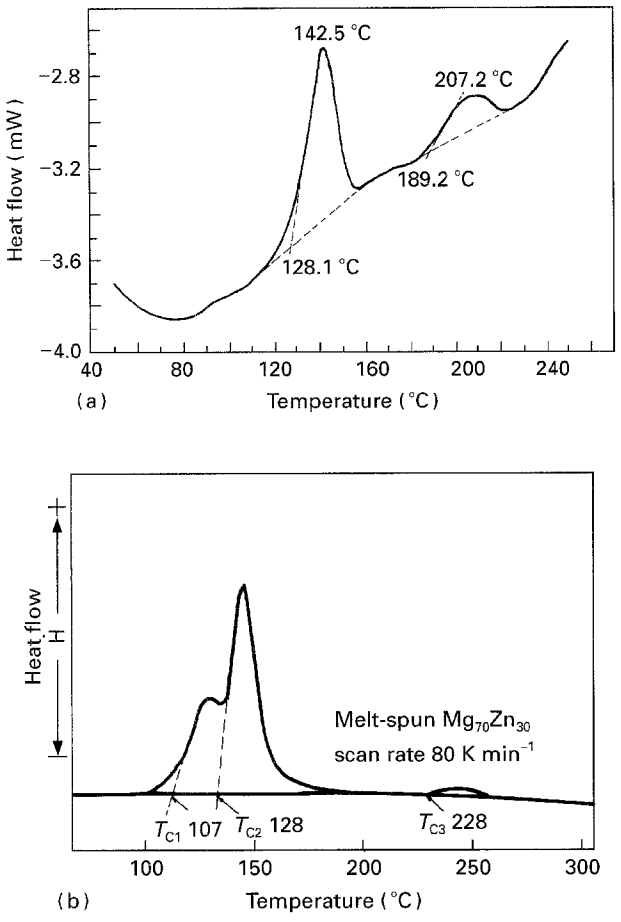

Figure 8 DSC thermograms of (a) rapidly solidified Zn–6 wt % Mg alloy on heating, showing precipitation reactions in the solid state, (b) amorphous $Mg_{70}Zn_{30}$ [3].

The present results, in agreement with previous work [5–10], show that under normal solidification conditions (but still non-equilibrium), the metastable eutectic mixture, Zn–$MgZn_2$ (EU1), forms in zinc-rich Zn–Mg alloys with its characteristic spiral morphology. Although rapid solidification of metallic alloys is known to produce metastable phases in many cases, contrary to this prediction, the equilibrium eutectic mixture of Zn–Mg_2Zn_{11} was observed in rapidly solidified Zn–Mg alloys. This anomalous behaviour may be explained on the basis of the requirement of maintaining an orientation relationship which usually exists between the two phases during eutectic solidification. The orientation relationship of Zn–$MgZn_2$ (EU1) [9] and Zn–Mg_2Zn_{11} (EU2) [8] eutectic have been studied, and it was postulated [20] that the formation of the EU2 structure requires cellular growth of a eutectic phase to satisfy this orientation relationship. This necessitates, in the presence of large compositional boundary layers, the instability of the interface which is analogous to, but more complex than, that which leads to cellular instabilities in single-phase materials. In the present case, it seems likely that such instability conditions are met in the rapidly solidified Zn–Mg alloys. Interface breakdown can readily occur as the growth rate changes across the ribbon thickness to give two-phase instability in the form of eutectic cells (Fig. 7a) and the single-phase instability of the EU2 structure which is associated with the structural transition from EU2 to a well-defined band of primary zinc dendrites (Fig. 7b). It appears that the interface stability and the asymmetric nature of the coupled zone play a major role in the selection of eutectic mixtures in zinc-rich Zn–Mg alloys under rapid solidification conditions.

4. Conclusions

1. In zinc-rich Zn–Mg alloys, the metastable eutectic mixture (EU1) forms under normal solidification conditions, whereas the equilibrium, stable eutectic structures (EU2) are observed after rapid solidification. The extent to which a specific microstructure is present in rapidly solidified Zn–Mg alloys has been described by using a growth rate–composition map.

2. These alloys exhibited interesting eutectic phase selections and structural transitions across the ribbon thickness, which appears to be a function of growth rate and interface instability.

3. In eutectic and hypereutectic alloys, a critical growth rate seems to exist beyond which eutectic solidification is not possible, suggesting possible transition from eutectic solidification to amorphous phase formation that subsequently crystallizes on cooling.

Acknowledgement

The authors thank Fry's Metals Ltd, for supporting this work.

References

1. J. W. CAHN, in "Proceedings of the Rapid Solidification Processing: Principles and Technologies II", edited by R. Mehrabian, B. H. Kear and M. Cohen (Claitor's, Baton Rouge, LA, 1980) p. 24.
2. H. JONES, *Mater. Sci. Eng.* **A133** (1991) 33.
3. A. CALKA, M. MADHAYA, D. E. POLK, B. C. GIESSEN, H. MATYJA and J. VANDERSANDE, *Scripta Metall.* **11** (1977) 65.
4. P. G. BOSWELL, *Mater. Sci. Eng.* **34** (1978) 1.
5. H. Y. LIU and H. JONES, *Acta Metall.* **40** (1992) 229.
6. R. L. FULLMAN and D. L. WOOD, *ibid.* **2** (1954) 188.
7. J. D. HUNT and J. P. CHILTON, *J. Inst. Metals* **94** (1966) 146.
8. R. R. JONES and R. W. KRAFT, *Trans. Met. Soc. AIME* **242** (1968) 1891.
9. A. DIPPENAAR and H. D. W. BRIDGMAN and G. A. CHADWICK, *J. Inst. Metals.* **99** (1971) 137.
10. M. N. CROKER, D. BARAGAR and R. W. SMITH, *J. Crystal Growth* **30** (1975) 198.
11. T. B. MASSALSKI, L. F. VASSAMILET and Y. BIENVENU, *Acta Metall.* **21** (1973) 649.
12. W. J. BOETTINGER, F. S. BIANCANIELLO, G. M. KALONJI and J. W. CAHN, in "Proceedings of the Rapid Solidification Processing: Principles and Technologies II", edited by R. Mehrabian, B. H. Kear and M. Cohen (Claitor's Baton Rouge, LA, 1980) p. 50.
13. J. W. CAHN, S. R. CORIELL and W. J. BOETTINGER, in "Proceedings of the Laser and Electron Beam Processing of Materials", edited by C. W. White and P. S. Peercy (Academic Press, New York, 1980) p. 89.
14. J. BOETTINGER, in "Rapidly Solidified Amorphous and Crystalline Alloys", edited by B. H. Kear, B. C. Giessen and M. Cohen (Elsevier, New York, 1982) p. 15.

15. M. V. AKDENIZ, PhD thesis, The Open University, Milton Keynes (1989).
16. T. W. CLYNE, *Metal. Trans.* **15B** (1984) 369.
17. H. E. CLINE, *J. Appl. Phys.* **53** (1982) 4896.
18. W. J. BOETTINGER, D. SCHECHTMAN, R. J. SCHAEFER and F. S. BIANCANIELLO, *Metall. Trans.* **15A** (1984) 55.
19. R. TRIVEDI, P. MAGNIN and W. KURZ, *Acta Metall.* **35** (1987) 971.
20. J. D. HUNT and D. T. J. HURLE, *Trans. Met. Soc. AIME* **242** (1968) 1043.

Received 22 February 1994
and accepted 11 April 1995